Res Chem Intermed (2015) 41:7299–7311
DOI 10.1007/s11164-014-1813-4

Enhanced visible light-induced hydrophilicity in sol–gel-derived Ag–TiO_2 hybrid nanolayers

Ali Akbar Ashkarran · Mahshid Ghavamipour · Habib Hamidinezhad · Hedayat Haddadi

Received: 29 April 2014 / Accepted: 15 September 2014 / Published online: 8 October 2014

Abstract Silver-doped TiO_2 hybrid nanolayers (NLs) were prepared via the sol–gel method using $TiCl_4$ as a precursor, and the products were characterized by X-ray diffraction, atomic force microscopy, scanning electron microscopy, transmission electron microscopy, and X-ray photoelectron spectroscopy. A detailed study of the visible light hydrophilicity of Ag–TiO_2 NLs by evaluating the contact angle of water droplets on the surface of the layers has been performed. Furthermore, a series of experiments was carried out in order to find the optimum value of dopant concentration. The results revealed that the Ag–TiO_2 hybrid NLs extended the light absorption spectrum toward the visible region and considerably enhanced the hydrophilicity of TiO_2 NLs under visible light irradiation. The significant enhancement in the visible light hydrophilicity activity of TiO_2 NLs under visible light irradiation can be ascribed to the generation of a new electronic state acting as an electron trap in TiO_2 and responsible for narrowing the band gap of TiO_2 and shifting its optical response from the ultraviolet to the visible light region.

Keywords Ag–TiO_2 · Hybrid nanolayers · Sol–gel · Visible light · Hydrophilicity

A. A. Ashkarran (✉)
Department of Physics, Faculty of Basic Sciences, University of Mazandaran, Babolsar, Iran
e-mail: ashkarran@umz.ac.ir

M. Ghavamipour
Department of Physics, Alzahra University, P.O. Box 1993891176, Tehran, Iran

H. Hamidinezhad
Department of Basic Sciences, Sari Agricultural Sciences and Natural Resources University, P.O. Box 578, Sari, Iran

H. Haddadi
Department of Chemistry, Faculty of Sciences, Shahrekord University, P.O. Box 115, Shahrekord, Iran

Introduction

Titanium dioxide has been extensively utilized as an efficient photocatalytic material in decomposing toxic organic molecules to H_2O, CO_2 and other non-toxic molecules [1, 2]. This property has also been applied in the inactivation of bacteria and hazardous components from water and air, as well as in self-cleaning or self-sterilizing surfaces for places such as medical centers [3, 4]. Specifically, much interest has been shown towards its super-hydrophilicity property in recent years since Wang et al. [5] discovered the photoinduced super-hydrophilicity of TiO_2 thin films in 1997. A surface coated with a TiO_2 layer exhibits an extremely high affinity for water when exposed to ultraviolet (UV) light and the contact angle decreases to almost zero. This property gives self-cleaning and antifogging effects to the coated surface and has already been applied to some construction materials [6, 7]. Conventional TiO2 hybrid nanolayers (NLs) require UV irradiation for effective hydrophilicity. Consequently, it is limited in practical applications because only 4 % of the solar spectrum is composed of UV illumination. [8]. In this regard, researchers have been interested in the modification of electronic and optical properties of this semiconductor for its efficient use under visible light irradiation [9, 10].

Approaches for making TiO_2 active in the visible light region are usually categorized into three main classifications: doping TiO_2 with transition metal ions such as V, Cr, Mn, Fe, Ag, Co, Ni; doping nitrogen into TiO_2; and coupling of TiO_2 with a small band-gap semiconductor which extends light absorption into the visible region [2].

Many reports have presented in nitrogen-doped TiO_2 as an efficient visible light-active TiO_2 [9, 11–18]. Nitrogen doping into the TiO_2 matrix is more favorable due to its similar atomic size as oxygen, small ionization energy, metastable center formation and stability. The substitution of nitrogen modifies both the electronic properties and the surface structure of TiO_2, where the former determines the light response range and redox power of the carriers, and the latter controls the surface transfer of the charge carriers [3]. Sn and Nb co-doped TiO_2 were coated on glazed porcelain substrates via sol–gel and dip-coating methods by Kaleji and Hosseinabadi [19]. The wettability results indicated that Sn and Nb dopant ions had significant effects on the hydrophilicity property of TiO_2 thin films under visible light irradiation. In a similar study, Mokhtarimehr et al. [20] also found that vanadium as a dopant ion had a significant effect on the hydrophilicity property of vanadium-doped TiO_2–SiO_2 thin films both under UV and visible light irradiation.

On the other hand, silver may also act as a suitable option for the synthesis of visible light-active hydrophil layers since many studies are investigating the synthesis of silver-doped TiO_2 as an efficient visible light-active photocatalyst [21, 22]. Hamal et al. [4] found that Ag–TiO_2 NPs, achieved by the sol–gel route, degrade the gaseous acetaldehyde ten times faster than commercial TiO_2 (Degussa P25) under visible light. Ag/$InVO_4$–TiO_2 thin films were developed through the sol–gel method from the TiO_2 sol containing Ag and $InVO_4$ by Ge and co-workers. It has been confirmed that the Ag/$InVO_4$–TiO_2 thin films can be excited by visible light (i.e. $E_g < 3.2$ eV). The significant enhancement in the Ag/$InVO_4$–TiO_2 photo-

activity under visible light irradiation can be ascribed to the simultaneous effects of doped noble metal Ag acting as electron traps and $InVO_4$ as a narrow band gap sensitizer [23]. It is known that there is a direct relationship between the photocatalytic activity and the photo-induced hydrophilicity of TiO_2. Therefore, we may conclude that superior photocatalyst materials are usually also good hydrophil layers [24].

In this work, we prepare visible light-active Ag–TiO_2 hybrid NLs using a single doping process via sol–gel and spin-coating methods. We have studied the influence of different dopant concentrations on the hydrophilicity of the produced TiO_2 NLs under visible light irradiation. Also, the amount of optimum silver on the hydrophilicity performance of TiO_2 NLs was investigated.

Experimental details

Synthesis of TiO_2 NLs

The schematic diagram of the synthesis procedure which includes two parts is shown in Fig. 1. The sol–gel process was used to synthesize TiO_2 NLs. An amount of 1 mL $TiCl_4$ (99 %; Merck) was slowly added dropwise into 10 mL ethanol (99.8 %; Merck) under vigorous stirring at room temperature. A large amount of HCl gas was exhausted and a transparent yellowish solution was formed. Soda lime glass ($25 \times 40 \times 2$ mm^3) was applied as substrate. Before the coating process, all substrates were cleaned with acetone, HCl 0.2 M, distilled water and, finally, by an ultrasonic (30 kHz, for 15 min.). The substrates were then spin-coated at 12,000 rpm in air and at room temperature using the as-prepared sol. Then, the obtained layers were dried at 100 °C for 1 h and annealed at 450 °C in air for another 1 h. To obtain TiO_2 nanopowders, the dried sol was annealed at 450 °C in air for 1 h.

Synthesis of Ag–TiO_2 hybrid NLs

For synthesis of Ag–TiO_2 hybrid NLs, different concentrations of silver solution (0.001, 0.01, 0.1, 1 and 10 mM), using $AgNO_3$ as a silver source, were prepared in ethanol. An amount of 1 mL $TiCl_4$ was slowly added dropwise into a fresh 10 mL silver solution with the desired concentration under vigorous stirring at room temperature. The obtained solution was then irradiated with a 2-mW cm^{-2} UV light source using a 125W high-pressure mercury lamp with 365 nm as the strongest wavelength for 2 h. This solution was used for spin coating on glass substrates at 12,000 rpm in air and at room temperature. Finally, the obtained layers were dried at 100 °C for 1 h and annealed at 450 °C in air for another 1 h. To obtain Ag–TiO_2 nanopowders, the dried sol was annealed at 450 °C in air for 1 h.

Characterization

Analysis of the crystalline structures was performed by X-ray diffraction (XRD) diffractometer (X'pert Philips) with the wavelength of Cu Kα radiation in the 2θ

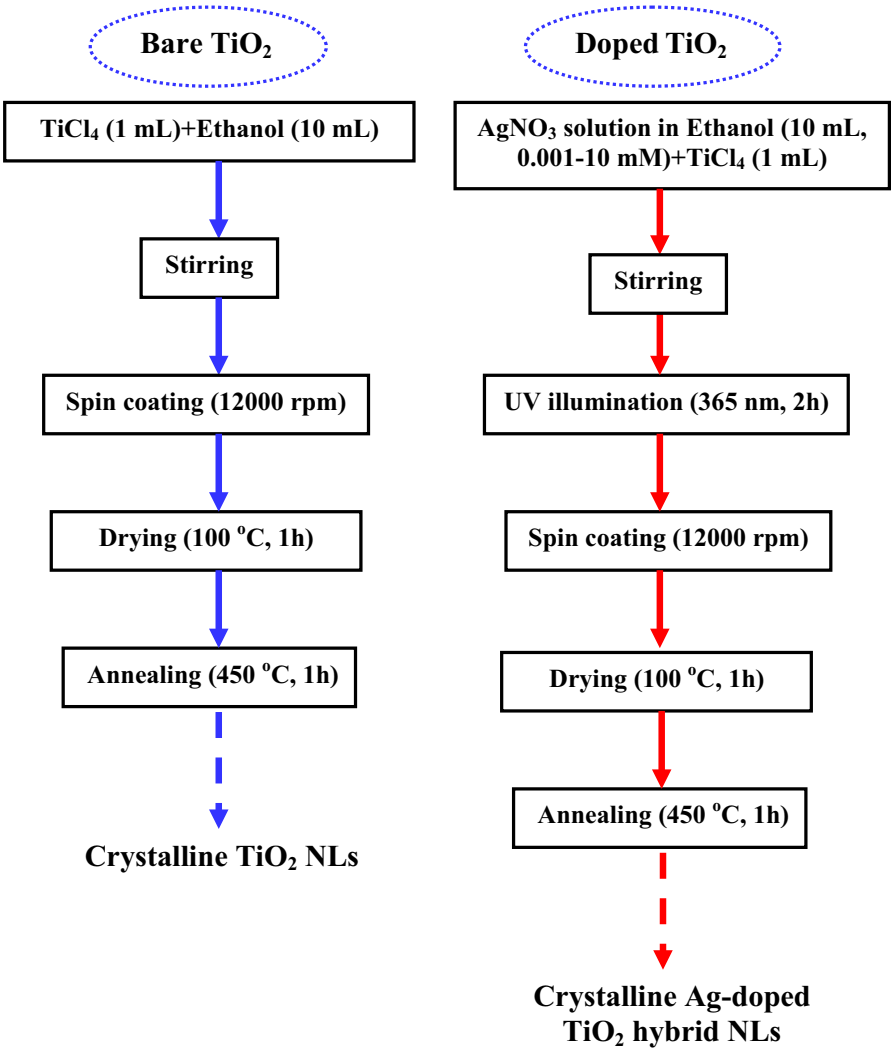

Fig. 1 Schematic diagram showing the procedure for synthesis of bare TiO_2 and Ag–TiO_2 hybrid NLs

range from 10° to 80° by 0.005° s^{-1} steps. X-ray photoelectron spectroscopy (XPS) analysis was carried out by a double Mg–Al anode X-ray source. A concentric hemispherical analyzer (model EA10 plus; Specs) was employed to analyze the emitted electrons from the surface. The energy axis was calibrated by adjusting the carbon peaks at 285 eV. Atomic force microscopy (AFM) images were captured by a Veeco Autoprobe instrument in non-contact mode, and the results were analyzed by Spip software (v.6.2.6). Scanning electron microscopy (SEM) analysis was carried out by a SEM instrument (Philips XL30) at 10–20 keV accelerating energy. Transmission electron microscopy (TEM) analysis was performed by a LEO 912

AB instrument at 100–200 keV accelerating energy by deposition of nanostructures onto the copper grid at room temperature.

Hydrophilicity study

Hydrophilicity of the bare TiO_2 and Ag–TiO_2 hybrid NLs was investigated by measuring the contact angle of DI water droplets on the surface of the TiO_2 NLs by a data physics OCA 15 plus contact angle meter under visible light irradiation using a 90-W halogen lamp. The distance between lamp and surface of the samples was 3 cm in all experiments. Five measurements were performed with the same sample in ambient air with droplets of about 3 mm diameter, and the average contact angel value was considered as final data.

Results and discussion

XRD analysis of the products

XRD analysis was carried out to find the crystalline phase and structure of the formed layers. The results for pure TiO_2 and silver-doped TiO_2 are illustrated in Fig. 2. The XRD pattern of the as-prepared NLs (Fig. 2a) shows the formation of crystalline TiO_2 in anatase phase. The strongest peak at $2\theta = 25.3°$ is representative for (1 0 1) anatase phase reflections. The obtained spectrum has the TiO_2 anatase phase peaks at $2\theta = 25.3, 37.7, 47.8, 54, 62.7$ and $75.2°$ with no impurity, which is in agreement with the 21-1272 standard card from JCPDS [25]. Figure 2b shows the XRD results of the 0.01 mM silver-doped TiO_2. It was observed that doping silver into the TiO_2 matrix leads to the formation of Ag_2TiO_3, Ag_2O and Ag phases in addition to anatase. The peaks appearing at $2\theta = 30.7$, 41.4, and $42.6°$ correspond to the formation of Ag_2TiO_3, $2\theta = 33.1$ corresponds to the formation of Ag_2O, and $2\theta = 35.6$ corresponds to the formation of Ag phases, according to the 41-1104, 1104 and 0783 standard cards from JCDPS, respectively. Substitution of silver for Ti^{4+} should result in a corresponding peak shift in the XRD, but no obvious shift for the diffraction peaks of TiO_2 was observed, indicating that no solid solution between the dopant and the host matrix was formed. The absence of such shifts in the recorded XRD indicates the segregation of dopants in the grain boundaries of TiO_2, or the incorporation of only an insignificant quantity in the substitutional Ti sites. In addition, as Yu et al. [26] reported, a solid solution occurs when the concentration of doping is so low that it is not detectable by XRD. This was while we observed the formation of a combination phase of silver and titanium in the Ag-doped TiO_2 samples. Consequently, the dopant probably did not enter into the crystal structure of titania to form a solid solution as was also confirmed by XPS analysis.

XPS analysis

To be certain about the composition of the products, we performed XPS analysis. Figure 3 shows the full survey XPS data for the 0.01 mM Ag-doped TiO_2 samples. From

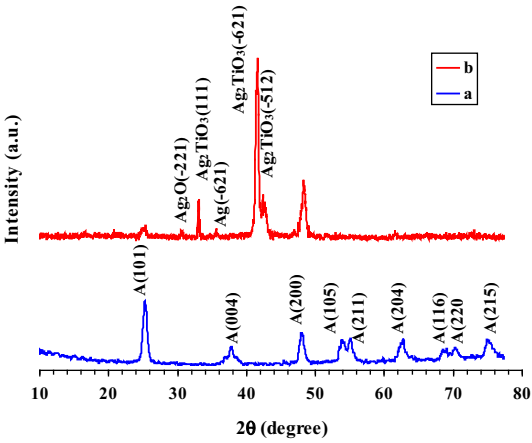

Fig. 2 XRD pattern of (*a*) bare and (*b*) 0.01 mM Ag-doped TiO_2 NLs

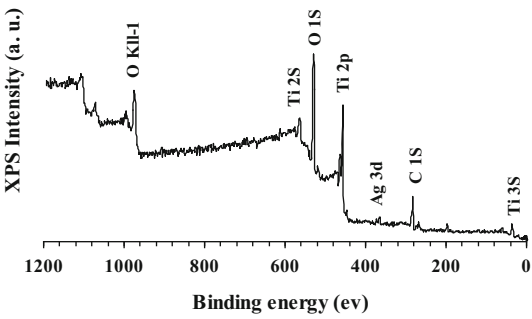

Fig. 3 Full survey XPS data of 0.01 mM Ag-doped TiO_2 NLs

the XPS spectrum, the binding energies of O 1s, Ti $2p_{3/2}$ and Ti $2p_{1/2}$ are 530.4, 459.7 and 465.8 eV, respectively. In addition, a weak C 1s peak at 285 eV is observed due to ambient air contamination. The O 1s peak (Fig. 4a) is located at 530.4 eV, indicating typical metal oxides (centered at 528.1–531.0 eV). The result for the Ag-doped TiO_2 also reveals the formation of Ag 3d. The O 1s XPS spectrum in Fig. 4a verifies the formation of the Ti–O–Ag structures, consistent with the reported values for Ag-doped titania NLs [27]. High-resolution XPS analysis in the range of titanium and silver binding energies is illustrated in Fig. 4b, c. Ag $3d_{5/2}$ and Ag $d_{3/2}$ peaks were observed at 367.7 and 373.9 eV, respectively, which are in agreement with literature values. The peak around 368 eV is assigned to adsorbed molecules as silver oxides such as AOx in the form of Ti–O–Ag linkage, which is generally named interstitial silver [28].

Microscopic studies

Surface morphology and roughness are two fundamental factors in the hydrophilicity of TiO_2 NLs. Figure 5 shows 2D AFM images and the corresponding size distributions of the layers prepared at different silver concentrations. The results show that, by increasing the dopant concentration from 0 to 0.01 mM, the average

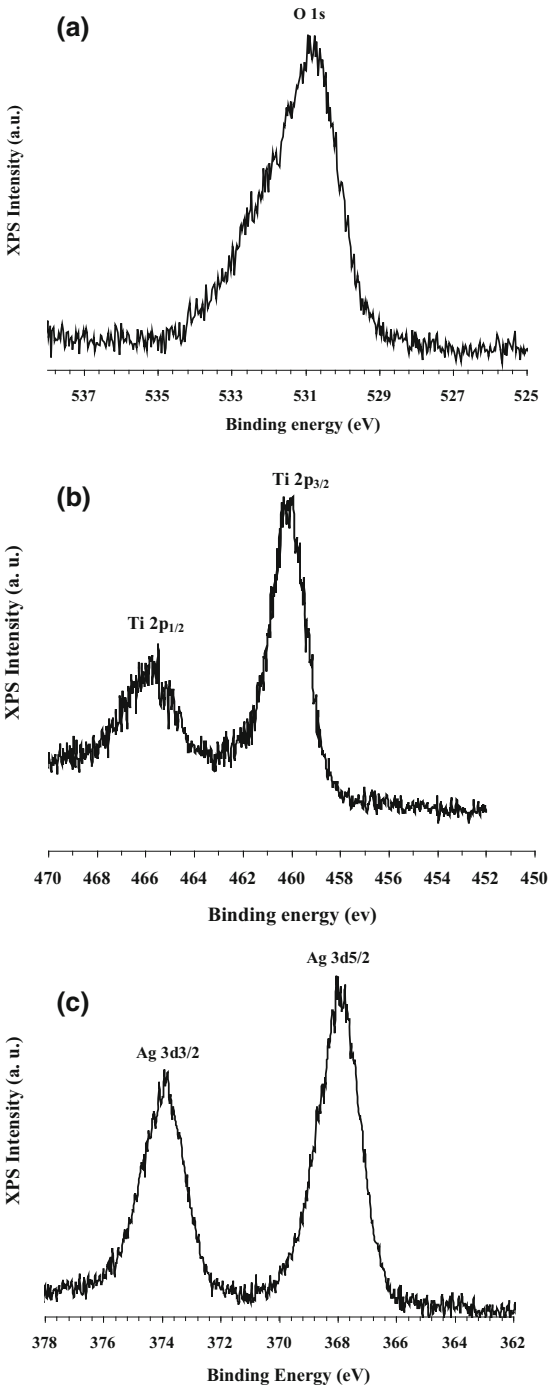

Fig. 4 High resolution XPS data in the range of **a** oxygen, **b** titanium and **c** silver binding energies

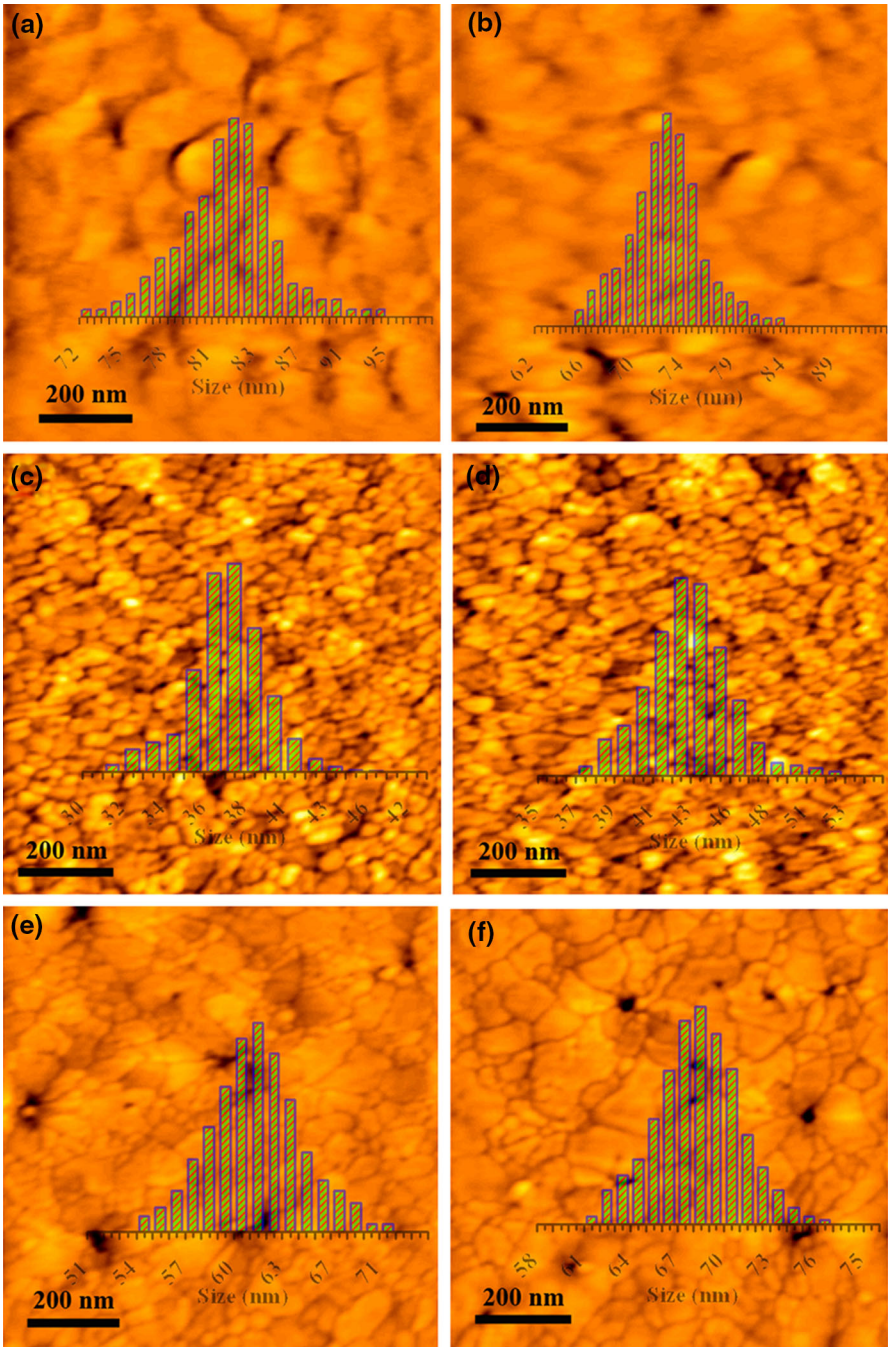

Fig. 5 AFM images of TiO_2 NLs with various silver contents: **a** undoped, **b** 0.001, **c** 0.01, **d** 0.1, **e** 1 and **f** 10 mM Ag-doped TiO_2 (overlayed *bar graphs* are the corresponding size distributions obtained from AFM images)

Table 1 Average grain size and roughness of the TiO_2 NLs prepared at different dopant concentrations, calculated based on the AFM images

Dopant concentration	Average grain size (nm)	Average roughness (nm)	$\Delta\theta$ (degree)
0 (bare TiO_2)	81.8 ± 2.8	4.83	~3 ± 0.6
0.001	72.7 ± 2.6	3.74	~17.2 ± 1.5
0.01	36.4 ± 1.4	2.21	~21.3 ± 1.7
0.1	42.5 ± 1.7	2.52	~17.7 ± 1.5
1	61.2 ± 2.3	3.12	~17.1 ± 1.4
10	68.3 ± 2.5	3.89	~14.6 ± 1.1

grain size and roughness of the surface decreased but with a further increase in dopant concentration up to 10 mM, these values increased. These results indicate the critical effect of doping on grain size and roughness of the TiO_2 NLs. A summary of calculated average grain size and roughness of the TiO_2 NLs based on the AFM results is shown in Table 1. The average grain size of TiO_2 particles became smaller by silver doping which has also been reported by Mokhtarimehr et al. [20]. They found that doping the TiO_2 had a suppressive effect on the crystal growth of the titania, since the additives, available in the boundary region of the TiO_2 particles, reduce crystallite growth during the heat treatment. But, further increases in dopant concentration may cover the TiO_2 particles and as a result increase the particles size and surface roughness. It has been shown that, with a moderate surface roughness (i.e. <3), superwetting should be possible on any material having an intrinsic contact angle <60° [29]. Shape and size recognition are fairly difficult from the scanning electron microscope (SEM) analysis (see, for example, Fig. 6a) due to the agglomeration of particles, but TEM images provide more insight into the specific details of the nanostructures (for electron microscope images, the corresponding powder form of the desired sample was prepared.) Therefore, the size distribution and shape of nanostructures were characterized by TEM microscope. Nearly spherical NPs were found in TEM images of bare TiO_2 samples. The silver particles are too small to be observed by SEM but they are quite obvious in TEM images (dark dots in Fig. 6c). The black dots in the TiO_2 matrix which has also been reported in other studies can be attributed to the accumulation and the high electron density of silver NPs (see, for example, Ref. [30]).

Contact angel measurements

The average contact angle changes of water droplets on Ag–TiO_2 NLs are depicted in Fig. 7. The results show that the hydrophilicity performance of the TiO_2 surface depends on the silver concentration. It was observed that, by increasing the dopant concentration up to 0.01 mM, the average contact angle on the TiO_2 surface decreases, but, by further increasing the silver concentration, the average contact angle increases again. This means that there is an optimum value of dopant concentration in which the reduction in contact angle is at a maximum. Based on the obtained results, the optimum value of dopant concentration for the maximum

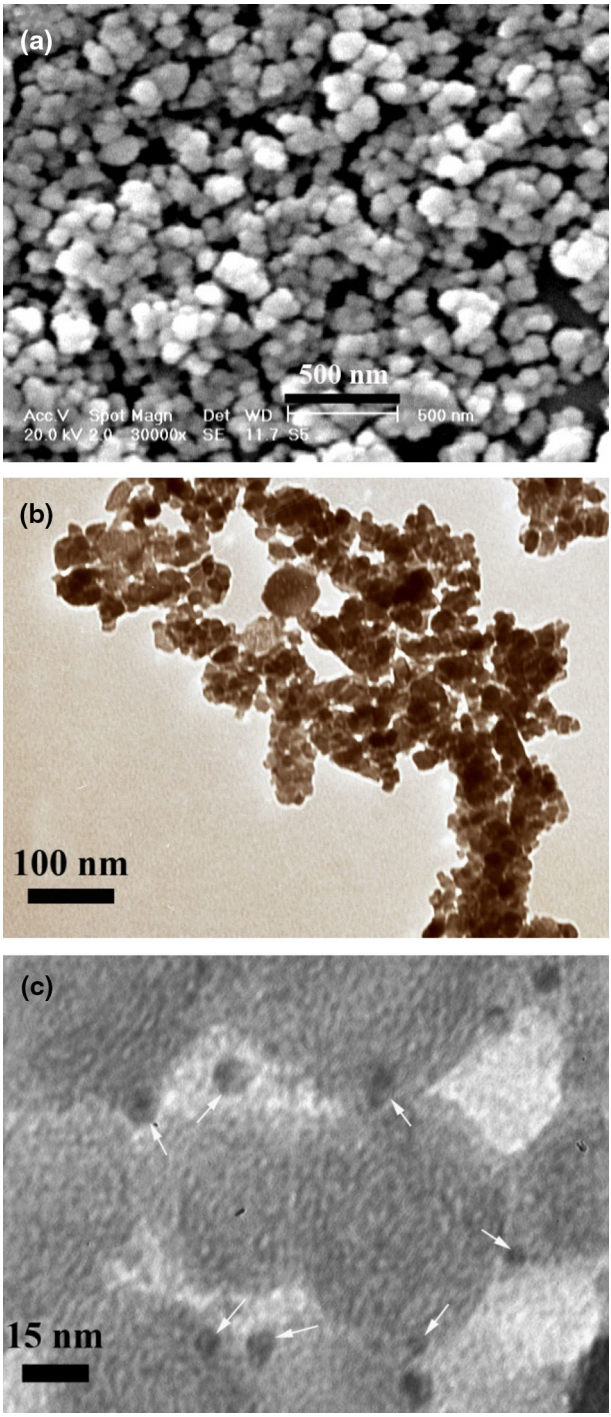
(a)
500 nm
Acc.V Spot Magn Det WD
20.0 kV 2.0 30000x SE 11.7 S5
500 nm
(b)
100 nm
(c)
15 nm

◀**Fig. 6** SEM image of **a** bare TiO_2 NPs, TEM image of **b** bare TiO_2 NPs and **c** 0.01 mM silver doped TiO_2 NPs (*arrows* indicate presence of silver NPs)

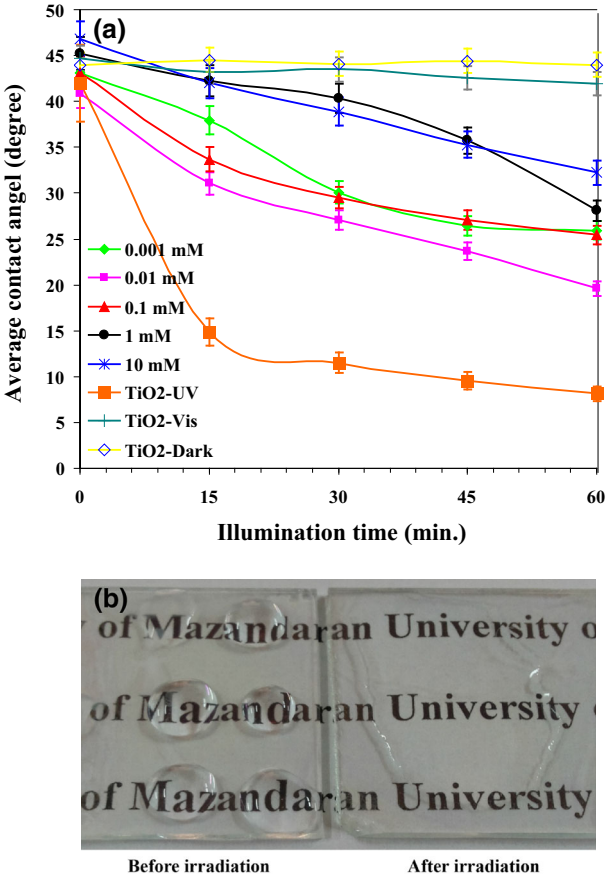

Fig. 7 **a** Changes in the contact angle of the water droplet under visible light irradiation on TiO_2 NLs with various silver contents and **b** optical image showing the hydrophilicity behavior of Ag–TiO_2 NLs before and after visible light irradiation

hydrophilicity under visible light irradiation may be 0.01 mM. No remarkable changes in the contact angle of water droplets on bare TiO_2 NLs were observed either in visible light irradiation or under dark condition (no light irradiation). Therefore, changes in contact angle under visible light illumination only depend on the photoexcitation of silver-doped-TiO_2 NLs.

Mechanism of silver-doped TiO_2 hydrophilicity

A schematic illustration of the modification of the band structure of TiO_2 due to silver doping is shown in Fig. 8. It is expected that doping silver can improve the

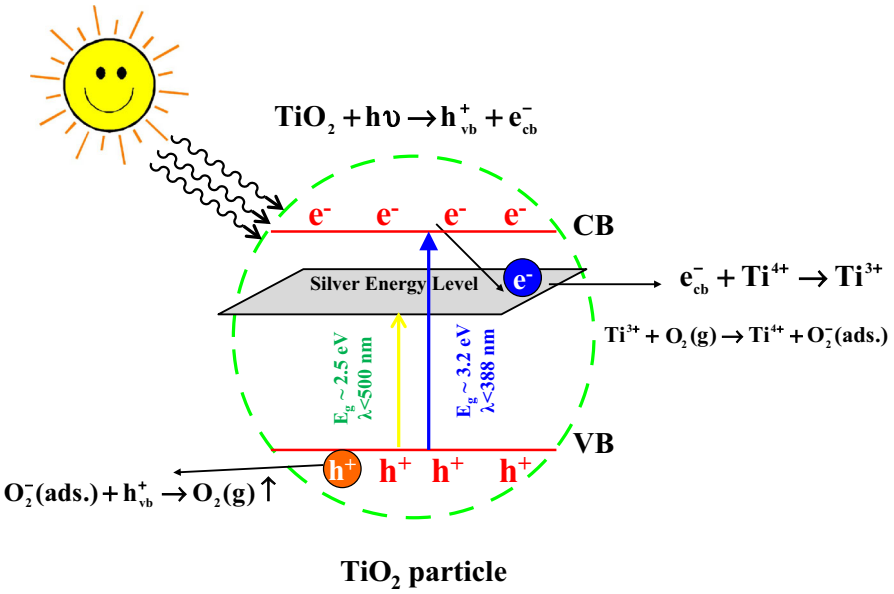

Fig. 8 Schematic illustration of the band structure of silver-doped TiO_2

hydrophilicity property of TiO_2 NLs under visible light irradiation since Ag can modify the band structure of TiO_2 by creating some energy levels within the band gap of TiO_2. Therefore, a reduction in band gap energy occurs, which leads to a narrower band gap and enhancement of the visible light absorption. In fact, silver doping introduces some new electronic states in the band gap of TiO_2, which increase the lifetime of the charge carriers [31]. At low concentrations, there are fewer trapping states while at higher dopant concentrations the number of trap levels increases and the average distance between the trap level decreases. Consequently, there is an optimum amount of dopant to rapidly trap electrons, but too much dopant may cover the titanium dioxide and prevent light absorption [32]. Moreover, too much dopant concentration may mean that the dopant acts as a recombination site itself and as a result leads to a decrease in photo-induced hydrophilicity efficiency [3].

Conclusion

We have prepared Ag-doped TiO_2 hybrid NLs using simple sol–gel and spin-coating methods with $TiCl_4$ as a precursor. XRD results demonstrated the coexistence of silver and TiO_2 phases, while the surface chemical composition of the NLs, determined by XPS, also showed the formation of silver and TiO_2. Hydrophilicity property of silver-doped TiO_2 NLs was probed by measuring the contact angle of water droplets on the TiO_2 surface both under dark condition and visible light irradiation. It was found that silver doping markedly affects the

hydrophilicity behavior of TiO_2 NLs under visible light irradiation. The doped TiO_2 NLs revealed a notable decrease in the contact angle of water droplets on the TiO_2 surface compared with undoped samples, which was concluded to be due to the band gap narrowing as a result of new generated energy levels within the TiO_2 band gap.

Acknowledgment Authors would like to thank Mr. Mohammad Reza Nourani for helping data analysis.

References

1. A. Fujishima, K. Honda, Nature **238**, 37 (1972)
2. J. Mo, Y. Zhang, Q. Xu, J.J. Lamson, R. Zhao, Atmos. Environ. **43**, 2229 (2009)
3. L.G. Devi, R. Kavitha, Appl. Catal. B **140–141**, 559 (2013)
4. D.B. Hamal, J.A. Haggstrom, G.L. Marchin, M.A. Ikenberry, K. Hohn, K.J. Klabunde, Langmuir **26**, 2805 (2010)
5. R. Wang, K. Hashimoto, A. Fujishima, M.E. Chinkuni, K.A. Kitamura, M. Shimohogoshi, T. Wanatabe, Nature **388**, 431 (1997)
6. X.L. Yuan, J.L. Zhang, M. Anpo, D.N. He, Res. Chem. Intermed. **36**, 83 (2010)
7. X. Feng, L. Jiang, Adv. Mater. **18**, 3063 (2006)
8. W. Zhu, D. Tong, J. Xu, Y. Liu, J. Ma, Thin Solid Films **526**, 201 (2012)
9. M. Anpo, Y. Ichihashi, M. Takeuchi, H. Yamashita, Res. Chem. Intermed. **24**, 143 (1998)
10. Y.K. Lai, J.Y. Huang, H.F. Zhang, V.P. Subramaniam, Y.X. Tang, D.G. Gong, L. Sundar, L. Sun, Z. Chen, C.J. Lin, J. Hazard. Mater. **184**, 855 (2010)
11. R. Asahi, T. Morikawa, T. Ohwaki, K. Aoki, Y. Taga, Science **293**, 269 (2001)
12. W. Buda, B. Czech, Water Sci. Technol. **68**, 1322 (2013)
13. Y. Cong, J. Zhang, F. Chen, M. Anpo, J. Phys. Chem. C **111**, 6976 (2007)
14. Y. Cong, J. Zhang, F. Chen, M. Anpo, D. He, J. Phys. Chem. C **111**, 10618 (2007)
15. Y. Cong, L. Xiao, J. Zhang, F. Chen, M. Anpo, Res. Chem. Intermed. **32**, 717 (2006)
16. T.C. Jagadale, S.P. Takale, R.S. Sonawane, H.M. Joshi, S.I. Patil, B.B. Kale, S.B. Ogale, J. Phys. Chem. C **112**, 14595 (2008)
17. G. Liu, Y. Zhao, C. Sun, F. Li, G.Q. Lu, H.M. Cheng, Angew. Chem. Int. Ed. **47**, 4516 (2008)
18. J. Lu, F. Su, Z. Huang, C. Zhang, Y. Liu, X. Ma, J. Gong, RSC Adv. **3**, 720 (2013)
19. B.K. Kaleji, N. Hosseinabadi, J. Sol–Gel Sci. Technol. (2013). doi:10.1007/s10971
20. M. Mokhtarimehr, M. Pakshir, A. Eshaghi, M.H. Shariat, Thin Solid Films **532**, 123 (2013)
21. F. Meng, F. Lu, J. Alloys Compd **501**, 154 (2010)
22. F. Meng, L. Xiao, Z. Sun, J. Alloys Compd **485**, 848 (2009)
23. L. Ge, M. Xu, H. Fang, J. Mol, A. Catal, Chem. **258**, 68 (2006)
24. M. Takeuchi, K. Sakamoto, G. Martra, S. Coluccia, M. Anpo, J. Phys. Chem. B **109**, 15422 (2005)
25. A.A. Ashkarran, M.R. Mohammadizadeh, Mater. Res. Bull. **43**, 522 (2008)
26. J. Yu, Q. Xiang, M. Zhou, Appl. Catal. B **90**, 595 (2009)
27. A. Zielinska, E. Kowalska, J.W. Sobczak, I. Lacka, M. Gazda, B. Ohtani, J. Hupka, A. Zaleska, Sep. Purif. Technol. **72**, 309 (2010)
28. S. Zhang, F. Peng, H. Wang, H. Yu, J. Yang, H. Zhao, Catal. Commun. **12**, 689 (2011)
29. J. Drelich, E. Chibowski, D.D. Meng, K. Terpilowski, Soft Matter **7**, 9804 (2011)
30. W. Su, S.S. Wei, S.Q. Hu, J.X. Tang, J. Hazard. Mater. **172**, 716 (2009)
31. M. Nasir, S. Bagwasi, Y. Jiao, F. Chen, B. Tian, J. Zhang, Chem. Eng. J. **236**, 388 (2014)
32. F. Meng, Z. Sun, Appl. Surf. Sci. **255**, 6715 (2009)